SALT-STRUCTURE INTERACTION OF UNDERGROUND NUCLEAR WASTE STORAGE

W. T. Li, N. J. Antonas, C. L. Wu, and K. M. Mark
Bechtel National, Inc., San Francisco, California 94119

ABSTRACT

This paper discusses the salt-structure interaction of the underground structures for the Waste Isolation Pilot Plant. The underground structures include the openings in the salt for shafts, drifts, and rooms, as well as the steel and concrete elements. This paper also summarizes the salt and structure behaviors as functions of time. An illustration is presented to show the chronological behavior of a typical structure, during construction and operating stages.

INTRODUCTION

The Waste Isolation Pilot Plant located in New Mexico is a research and development facility for defense related transuranic nuclear waste storage. The WIPP is designed to demonstrate the feasibility of permanent storage of this type of nuclear waste in a bedded salt formation.

In the storage facility, arrays of drifts, located 670m feet below ground, are mined in the salt formation. These drifts are connected to the surface by shafts. The drifts are used for the storage of the wastes, while the shafts are used to transfer the wastes from the surface and to support underground construction activities and ventilation requirements (Fig. 1).

The storage operation has two phases: the emplacement of the waste and the establishment of the permanent storage. Emplacement starts after the construction of the first storage drift, when the waste received in the surface handling structure is transferred to the storage level and stored in drifts. After the emplacement, the surface facilities are decommissioned, the storage area is backfilled, the shafts are sealed, and the storage site eventually becomes permanent[1].

In the design of waste storage in a salt formation, the objectives of both emplacement and decommissioning should be accomplished. Consequently, retrievability and encapsulation should be considered in the design in addition to conventional structural considerations, such as strength and stability. Salt creep studies are therefore required to predict the structural stability and the adequacy of the facility to perform the intended functions.

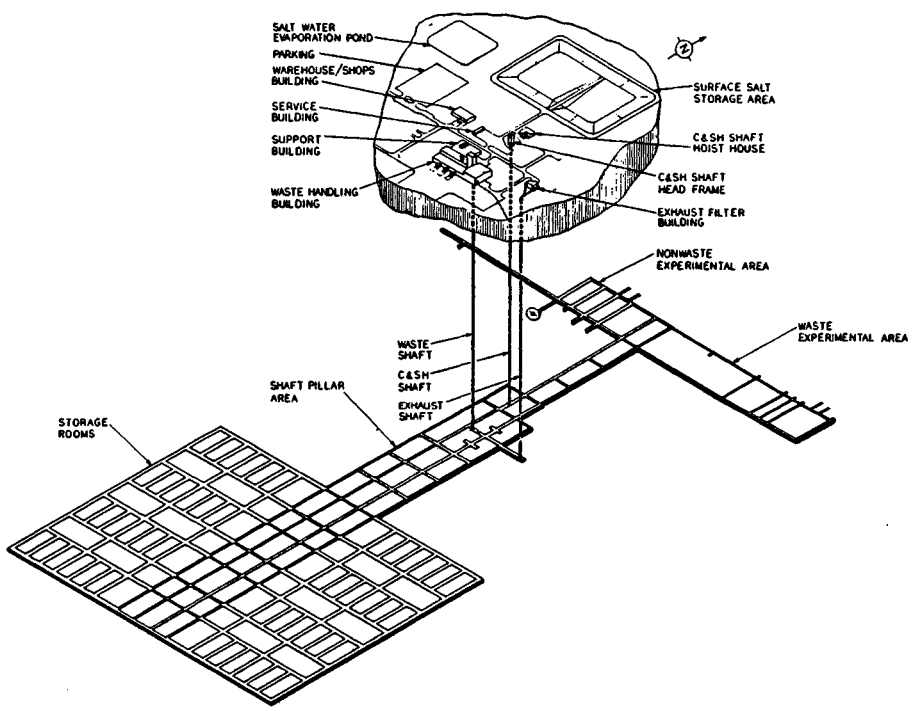

Fig. 1. Waste Isolation Pilot Plant

At present, there are two shafts open, namely, a 670.56m ventilation shaft, and a 701.04m exploratory shaft. The 3.66m diameter exploratory shaft has a steel liner to a depth of 256.64m, approximately 3m above the rock salt. This is followed by a 76.2 cm thick concrete ring (key) for an additional 12.19m, to prevent leakage of water from the upper aquifers into the salt formation and to anchor the lining into the rock (Fig. 2).

To verify the adequacy of the design and to study the phenomena of creep interaction between salt and structure, a non-linear creep analysis of the shaft key was performed[2,3].

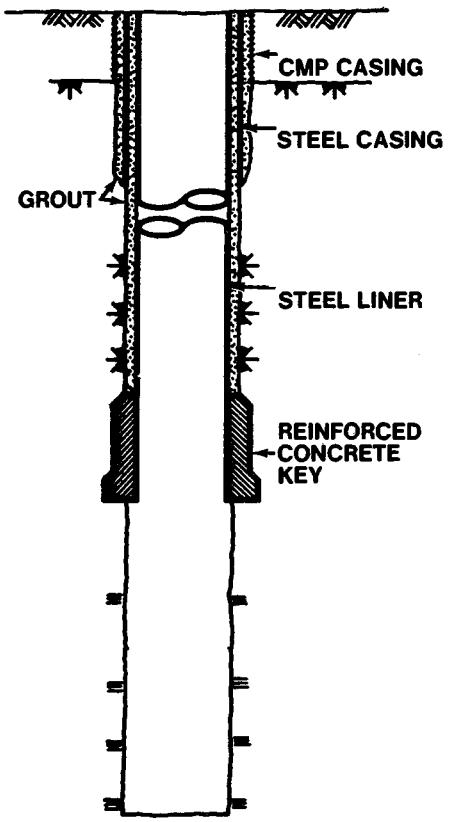

Fig. 2. Exploratory Shaft and Shaft Key

SALT PROPERTIES

Salt has the properties of adequate strength, low permeability, high thermal conductivity, and the capability of recrystallization, and can therefore provide an ideal geologic barrier between the waste and the biosphere. However, the most significant physical property of salt is that it creeps. The creep of the salt is dependent upon the stress, temperature, and time, and it occurs when the surroundings of the salt medium are disturbed. Stress distribution is determined by the lithostatic pressure and the configuration of storage areas. The configuration includes the dimensions of drifts, pillars, and shafts, as well as the extraction ratio. Temperature is a function of the heat generated from the waste and the volume of the waste with elevated temperature, while the time has to reflect the schedule of the excavation activities. In the WIPP facility where the storage area is deep below the surface, the high deviatoric stress due to excavation at great depths causes the salt to creep at a significantly high rate. This creep phenomenon, in turn, results in a redistribution of the stresses and the strains around the underground opening as time goes by. However, a facility requirement is that the closure process due to creep be slow enough so that the drifts remain open for a specified period of time in order that storage and retrieval of the waste can be made. After backfilling, the drift will eventually encapsulate the waste.

Geotechnical information was obtained from exploration holes and surface geophysical measurements. Moreover, extensive laboratory tests were performed, and the salt creep model was defined from the test results. From the geological study, it was found that the site stratigraphy consists of horizontal layers of halite, argillaceous halite, polyhalitic halite, anhydrite, polyhalite, and siltstone, with clay seams between some of these layers (Fig. 3).

The constitutive equation which describes the salt property was determined as follows:

$$\dot{\varepsilon}_{ij} = -\frac{\nu}{E}\dot{\sigma}_{kk}\,\delta_{ij} + \left(\frac{1+\nu}{E}\right)\dot{\sigma}_{ij} + \dot{\varepsilon}^{c}_{ij} + \alpha\,\dot{\theta}\,\delta_{ij}$$

where

$\dot{\varepsilon}_{ij}$ is the strain rate tensor

$\dot{\sigma}_{ij}$ is the stress rate tensor

E is Young's modulus

ν is Poisson's ratio

$\dot{\theta}$ is the temperature rate

α is the coefficient of linear thermal expansion, and

δ_{ij} is the Kronecker delta.

and the creep strain rate, $\dot{\varepsilon}^{c}_{ij}$, is given by

$$\dot{\varepsilon}^{c}_{ij} = |\dot{\varepsilon}^{c}_{kl}|\,\frac{\sigma'_{ij}}{|\sigma'_{mn}|}$$

where σ'_{ij} is the deviatoric stress tensor and

$$|\dot{\varepsilon}^{c}_{ij}| = \sqrt{1.5}\,\dot{\bar{\varepsilon}}$$

The effective creep strain rate $\dot{\bar{\varepsilon}}$ is defined as

$$\dot{\bar{\varepsilon}} = \left(\frac{2}{3}\dot{\varepsilon}^{c}_{ij}\,\dot{\varepsilon}^{c}_{ij}\right)^{1/2}$$

which is the sum of the primary and secondary creep strain rate, namely

$$\dot{\bar{\varepsilon}} = \dot{\bar{\varepsilon}}_p + \dot{\bar{\varepsilon}}_s$$

where $\dot{\varepsilon}_p$ can be defined by

$$\dot{\varepsilon}_p = (A - B\,\varepsilon_p)\,\dot{\varepsilon}_s \quad \text{for } \dot{\varepsilon}_s \geq \dot{\varepsilon}^{*}$$

and

$$\dot{\varepsilon}_p = \left(A - B\,\frac{\dot{\varepsilon}^{*}}{\dot{\varepsilon}_s}\,\varepsilon_p\right)\dot{\varepsilon}_s \quad \text{for } \dot{\varepsilon}_s < \dot{\varepsilon}^{*}$$

where A, B, and $\dot{\varepsilon}_s^*$ are the primary creep constants and $\dot{\varepsilon}_s$ can be defined by an exponential law

$$\dot{\varepsilon}_s = D\,\bar{\sigma}^n\, e^{-Q/R\theta}$$

where

$\bar{\sigma} = \left(\frac{3}{2}\sigma'_{ij}\,\sigma'_{ij}\right)^{1/2}$ is the effective stress

D, n are constants determined from data analysis

θ is the temperature

Q is the effective activation energy, and

R is the universal gas constant.

Load tests were also performed for the geologic deposits other than halite near the storage horizon. It was found that anhydrite, polyhalite, and siltstone are elastic, and their stress-strain relationship can be expressed by the linear-elastic constitutive equation

$$\varepsilon_{ij} = -\frac{\nu}{E}\sigma_{kk}\,\delta_{ij} + \left(\frac{1+\nu}{E}\right)\sigma_{ij}$$

There are also thin layers of clay present between some of the deposit layers. These clay seams could allow relative slippage and separation between the lithologic layers. Therefore, the creep behavior of the salt is also affected by the physical properties of the deposits adjacent to the salt and the discontinuity of geological planes near the storage location.

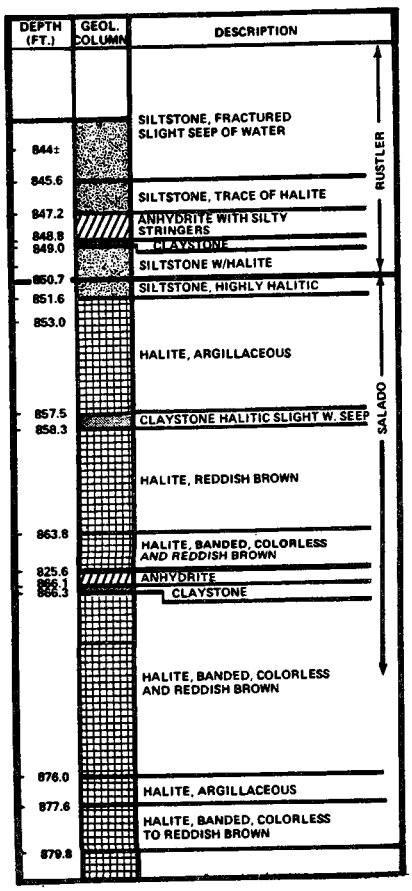

Fig. 3. Site Geologic Stratigraphy

STRUCTURE PROPERTIES

In addition to the existing salt, steel and concrete elements are used to strengthen the underground storage areas. For steel structures, since design stresses are below yield, only elastic behavior needs to be considered. But for concrete structures, effects due to the creep and shrinkage should also be considered. Both the creep and shrinkage of the concrete are related to the physical properties of the concrete, thickness and geometry of the structure, and the humidity of the environment.

The relationship for concrete shrinkage is of the form[3]

$$\varepsilon_{sh} = \frac{t}{3024000 + t}\,\varepsilon_{shu}\,C_{th}\,C_h\,C_s\,C_{cem}\,C_{fa}$$

where ε_{shu} is the ultimate shrinkage strain and C_{th}, C_h, C_s, C_{cem}, and C_{fa} are the correction factors for thickness, humidity, slump, cement, and percent fines and air content, respectively.

Beginning with the standard creep equation[4], the expression for creep, ε_c, became

$$\varepsilon_c = \frac{t^{0.6}}{9160.27 + t^{0.6}}\,\frac{\bar{\sigma}}{E}\,\varepsilon_{cu}\,C_{th}\,C_h\,C_s\,C_{la}\,C_{fa}$$

where ε_{cu} is the ultimate creep coefficient; t is the total creep time in seconds; C_{th}, C_h, C_s, C_{la} (loading age), and C_{fa} are the correction factors.

The standard creep relationship for concrete was developed from tests in which a constant load is applied to the concrete cylinders. Typically the creep relationship will be a function of the applied load and the modulus of elasticity will also change in time. As reported by Ross[5], the "rate of creep" method can reasonably predict the creep for widely varing states of stress, and a single creep curve with a single modulus of elasticity can be utilized.

After the concrete is placed, the shrinkage effect is more significant than the creep effect because of the low stress in the concrete. The rate of shrinkage strain decreases significantly after the first year.

INSTRUMENTATION

An instrumentation program is being conducted to confirm that the design of the facility meets the requirements for safety and operability. Rock mechanics instrumentation is installed during and after excavation operations. The main items of concern in the monitoring process are the geometric distortion of openings and adjacent rock, the rate of change of stress and strain gradients around openings, the in situ state of stress, the build up of hydrostatic pressure on the lined steel portion of the shaft, the salt creep pressure on the concrete shaft key, and the deformations of certain test facilities, such as the test pillar. The instruments used will typically be piezometers, earth pressure cells, strain gauges, extensometers, stressmeters and load cells. The entire instrumentation array will be monitored for a sufficient period of time to confirm the adequacy of

the analysis and consequent design of the facilities[6].

In order to measure interactive response between salt and structure, the piezometers were installed in the shaft, behind the steel lining at various elevations below the known acquifers down to the shaft key. The build up of hydrostatic water pressure on the lined portion of the shaft will be monitored to verify the predicted hydrostatic pressure and the adequacy of the lining design.

Also in the shaft key area, flexible flat jack type pressure cells were placed against the salt formation behind the concrete key wall. Two kinds of strain gauges were also installed, one embedded in concrete and another welded to the reinforcing steel. The lithostatic pressure due to salt creep and induced strain in the concrete key will be measured to validate the design of the key.

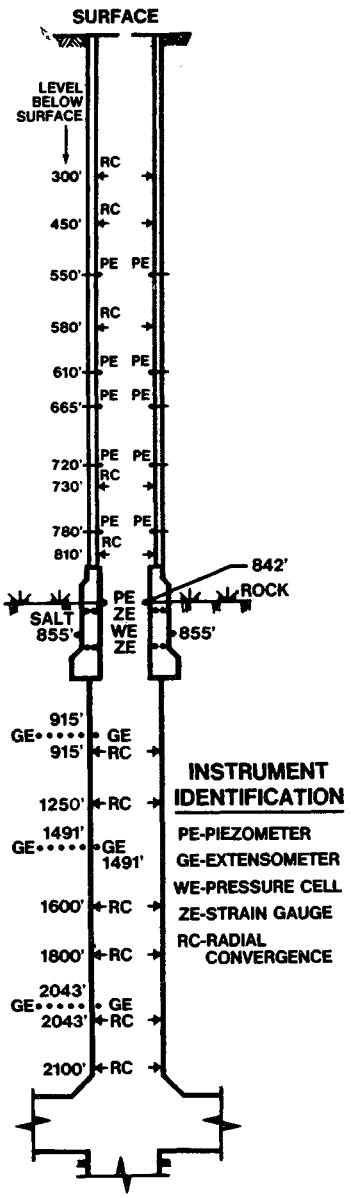

Fig. 4. Exploratory Shaft Instrumentation

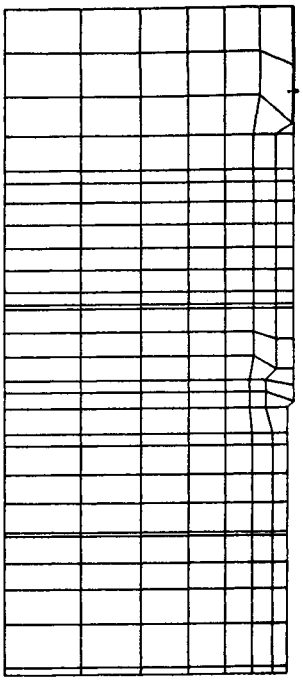

Fig. 5. Finite Element Model

Multi-point horizontal extensometers of 15.2m length with four anchor points were installed at various levels in the unlined salt portion of the shaft. Differential movements between the surface anchor and the anchors at depth will be measured to evaluate the geometric distorsion of the salt formation. Radial convergence points were also established at various elevations in the shaft for manual measurement of the deformation of the shaft wall (Fig. 4).

The geomechanical information gathered during the exploratory shaft program will be used in design of the additional required shafts for the full WIPP program.

SALT STRUCTURE INTERACTION

The structural behavior due to the effect of salt-structure interaction at different stages of time can be either measured or computed to evaluate the adequacy and operability of the structure. Since at this time, instrumentation measurements are not very extensive, interaction effects are determined by computational methods. Considering the complications of the geological conditions and the non-linear behavior of the salt, computer analysis using the finite element method is the best approach to obtain a reasonable result, even though computation of non-linear creep over a long time scale is costly.

An analysis of the shaft key was performed by finite element method using the MARC General Purpose Finite Element Analysis Program[7]. Figure 5 shows the finite element model of the creep analysis since both the shaft and the shaft key are symmetrical about the centerline of the shaft, quadrilateral axisymmetric ring elements are chosen for the model. The upper and lower boundaries were chosen at the elevations where the effects due to the excavation of the drifts were considered minimal.

The key and surrounding areas were modeled in detail, including 18 distinct geologic layers. To reduce the computation time, the stress and the strain at each integration point of the element were set equal to the respective values at the centroid of the element. Four clay seams at depths 258.74m, 261.49m, 264.02m, and 274.59m were considered as active slip planes, represented by friction and gap link elements. These elements provided frictional and gapping connection between any two nodes of a model. The element is based on imposition of gap closure constraint, frictional stick or slip via Lagrange's multipliers. The computations were made with a specified frictional coefficient of 0.4.

The boundary condition at the top of the model was a uniform pressure based upon the mass density of the geological formation from the surface of the ground to the elevation of the boundary. The vertical boundary of the model had zero horizontal displacement while the bottom boundary had zero vertical displacement.

The lithostatic stress state was assumed to be hydrostatic, i.e.,

$$\sigma_{xx} = \sigma_{yy} = \sigma_{zz} = -\int_0^y \rho \, dy$$

where ρ is the rock weight per unit volume, which is assumed to be a constant of 21252 kg/m^2-sec^2 and y is the depth in meters.

To overcome the problem of overly stiffened results due to the incompressibility constraints, a procedure of constant bulk pressure correction was used. [7] In this procedure, the bulk strain was calculated and added to the deviatoric strain at the centroid for each element.

The values of the elastic constants ν and E and the creep constants D, n and Q for the rocks are shown in Table I. The values of the correction factors for concrete creep and shrinkage are shown in Table II.

The analysis sequence was designed to duplicate actual construction sequences. Initially, the shaft surface was restrained to simulate the unexcavated condition. An internal stress was applied to simulate the initial lithostatic stress state, and the overburden pressure and unit weights were applied to compute the static solution[8]. The shaft surface restraints were then removed to simulate the excavation. The analysis was carried out for 5 years without the key, and a comparison of radial deformations was made to determine the time when creeping salt would come into contact with the shrinking concrete key. At that time, 2.67 years, the key was then actively tied to the model at the location of the key, and the analysis continued for a total of 30 years.

The analytical results showed that the stress distribution in the lithologic layers changed immediately after the excavation, and stress concentrations are formed around underground openings. From the time of initial contact, the average radial and hoop stresses in the key were increased and eventually reached values of, respectively, 1.413 MPa and 6.322 MPa, due to the increasing confining pressure of the creeping salt. Due to creep of the salt, the stresses are redistributed, relax quickly within one year, and decrease at a lower rate thereafter. After a year, there is not much change in the salt stresses.

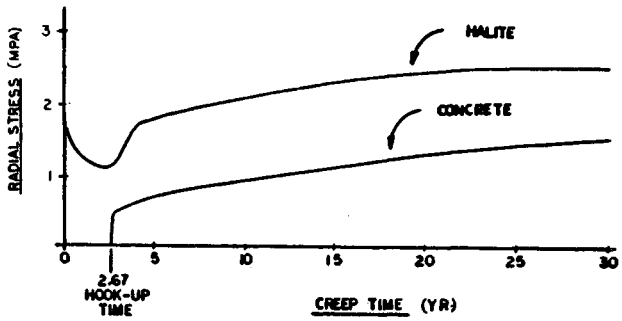

Fig. 6. Radial Stress Time Histories

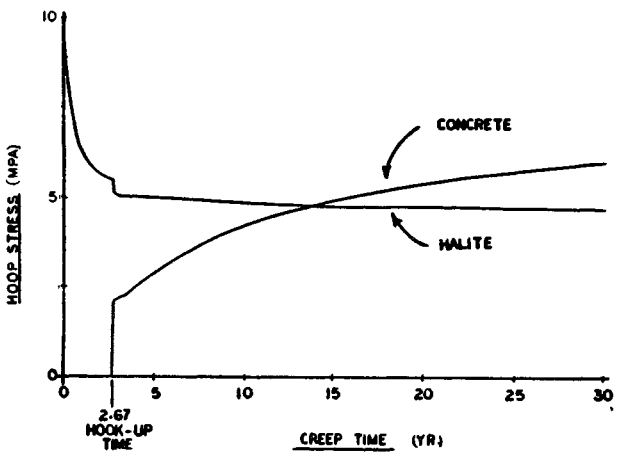

Fig. 7. Hoop Stress Time Histories

Material	ν	E	D	n	Q
		MPa	$Pa^{-4.9} \cdot s^{-1}$		$\frac{kcal}{mole}$
Halite	.25	31000	5.79×10^{-36}	4.9	12
Argillaceous halite	.25	31000	1.74×10^{-35}	4.9	12
Anhydrite	.35	75100	0.0	-	-
Siltstone	.20	3440	0.0	-	-

Table I. Material Properties of Rocks

	C_{th}	C_h	C_s	C_{cem}	C_{la}	C_{fa}	ε_{shu}	ε_{cu}
Shrinkage	.30	.900	1.050	.99	-	1.0	.0008	-
Creep	.59	.935	1.088	-	1.0	1.0	-	2.35

Table II. Factors for Concrete Shrinkage and Creep

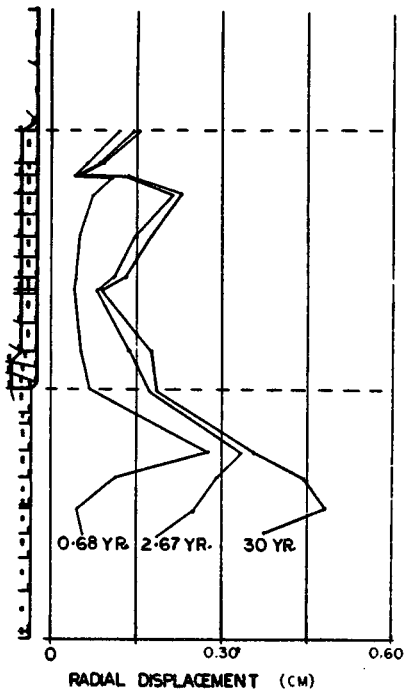

Fig. 8. Radial Displacement at Different Times

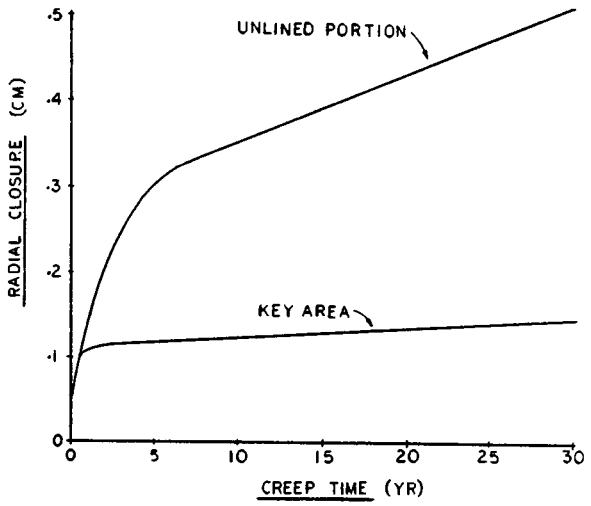

Fig. 9. Radial Closure Time Histories

However, due to the relaxation of the stress in the salt and the continuous deformation of the lithologic layers, more stresses are built up at certain locations in the deposits other than the salt. For the salt adjacent to the key, there was a similar increase in the radial stress, while the tangential stress was held approximately constant. Figures 6 and 7 show the time histories for the radial and hoop stresses, respectively, at the center points of adjacent concrete and salt elements. Maximum radial displacements of the key were on the order of 0.25 cm, approximately half the maximum radial displacement of the salt in the unlined portion of the shaft immediately below the key (Fig. 8).

The unbalanced state of the force due to the excavation of the shaft causes the lithologic layers to deform as well as slide and separate across the clay seams. The most important effect on the shaft is the closure of the shaft. The radial closure histories of the shaft at both the unlined portion and shaft key area from 0 to 30 years are shown in Figure 9. The closure rate was slow, starting at a rate of 0.09 cm/yr decreasing with the time, and approaching a constant of approximately 0.0007 cm/yr at the unlined portion and 0.001 cm/yr at the shaft key area. The radial closure of the shaft at 30 years was 0.50cm for the unlined portion and 0.14cm for the shaft key area.

CONCLUSION

The design of the WIPP incorporates state of the art design concepts, experience from similar minings, laboratory test data, analytical results, and in situ measurements. Instrumentation in the WIPP facility during and after the construction provides the information for the validation of the analytical results, and designs are refined as required to accomodate site-specific geological conditions. Correlation of this information will confirm the predicted analytical results, assure the adequancy of the design, and lead to further understanding of the methods of waste management in the area of underground storage technology.

REFERENCES

1. U.S. Department of Energy, Waste Isolation Pilot Plant Safety Analysis Report, (Sept. 1980).

2. W. T. Li, C. L. Wu, and N. Antonas, "Salt Creep Design Consideration for Underground Nuclear Waste Storage," Proc. of MRS 6th Int. Sym. on Scientific Basis for Nuclear Waste Management, (Nov., 1982).

3. N. J. Antonas, W. T. Li, K. M. S. Mark, C. L. Wu, "Creep Interaction of Salt and a Concrete Ring Structure", to be published in the Proceedings, ASCE EMD Specialty Conf., Purdue Univ., (May, 1983).

4. ACI Committee 209, "Prediction of Creep, Shrinkage, and Temperature Effects in Concrete Structure", ACI Publication SP27, (1971).

5. A. D. Ross, "Creep of Concrete Under Variable Stress", Journal of the ACI, (March, 1958).

6. J. W. Reum and E. V. Howes, "Geotechnical Instrumentation and Data Acquisition System for Site and Preliminary Design Validation at the DOE Waste Isolation Pilot Plant", IEEE Proc. on Nuclear Science, (Feb. 1982).

7. MARC Analysis Research Corp., "MARC General Purpose Finite Element Program User Information Manual," Rev. J.1, (1980).

8. W. T. Li and C. L. Wu, "Analysis of Creep for a Nuclear Waste Storage in Salt Formation," Nuclear Technology, (May, 1983).